Periodicity characterization of the nonlinear magnetization dynamics

Cite as: Chaos **30**, 093112 (2020); https://doi.org/10.1063/5.0006018
Submitted: 26 February 2020 . Accepted: 11 August 2020 . Published Online: 01 September 2020

J. A. Vélez, J. Bragard, L. M. Pérez, A. M. Cabanas, O. J. Suarez, D. Laroze, and H. L. Mancini

Chaos ARTICLE scitation.org/journal/cha

Periodicity characterization of the nonlinear magnetization dynamics

Cite as: Chaos 30, 093112 (2020); doi: 10.1063/5.0006018
Submitted: 26 February 2020 · Accepted: 11 August 2020 ·
Published Online: 1 September 2020

View Online Export Citation CrossMark

J. A. Vélez,[1] J. Bragard,[2] L. M. Pérez,[1,a)] A. M. Cabanas,[1] O. J. Suarez,[3] D. Laroze,[1] and H. L. Mancini[2,b)]

AFFILIATIONS

[1] Instituto de Alta Investigación, CEDENNA, Universidad de Tarapacá, Casilla 7D, Arica, Chile
[2] Departamento de Física y Matemáticas Aplicadas, Universidad de Navarra, Pamplona 31080, Spain
[3] Departamento de Física, Universidad de Sucre, A.A. 406 Sincelejo, Colombia

Note: This article is part of the Focus Issue, Instabilities and Nonequilibrium Structures.
[a)] **Author to whom correspondence should be addressed:** lperez@uta.cl
[b)] hectormancinimaza@gmail.com

ABSTRACT

In this work, we study numerically the periodicity of regular regions embedded in chaotic states for the case of an anisotropic magnetic particle. The particle is in the monodomain regime and subject to an applied magnetic field that depends on time. The dissipative Landau–Lifshitz–Gilbert equation models the particle. To perform the characterization, we compute several two-dimensional phase diagrams in the parameter space for the Lyapunov exponents and the isospikes. We observe multiple transitions among periodic states, revealing complex topological structures in the parameter space typical of dynamic systems. To show the finer details of the regular structures, iterative zooms are performed. In particular, we find islands of synchronization for the magnetization and the driven field and several shrimp structures with different periods.

Dissipative magnetization dynamics of parametrically driven anisotropic magnetic particles are analyzed. Our results show intricate dynamical behaviors. In particular, bi-stability, period-doubling bifurcations, chaotic states, as well as chaotic transients have been found. In the present article, we present a systematic study of the periodicity of the aforementioned system, through isospike diagrams. In addition, the largest Lyapunov exponent (LLE) and bifurcation diagrams are computed. We examine the effects of the external field and the particle's anisotropy.

I. INTRODUCTION

The characterization of periodicity and chaos is one of the most challenging tasks in nonlinear dynamical systems, and many techniques have been developed.[1–4] Commonly, the differentiation between chaotic and (quasi-)periodic states is given by the Lyapunov exponents.[5] Using this method, some topology structures of regular regions embedded in chaotic domains have been observed in two-dimensional parameter space, like shrimp, boomerangs, and the accumulations of both of them.[6,7] Since they have been found in several dynamical systems,[8–14] one can establish that there are robust phenomena. Therefore, a natural question arises about the structure of these (multi-)periodic regions. One novel method to numerically characterize the periodicity is the *isospike diagrams*.[15,16] This method measures the number of spikes per period of oscillation. Apart from the discrimination between chaotic and regular states, an isospike diagram reveals how the periodicity changes when the parameters are tuned, generating plenty of new information, which cannot be tracked by the Lyapunov exponent method. These diagrams have been applied in maps, electrical systems, chemical reactions, and convection in fluids, to name just a few.[17–30]

On the other hand, the magnetization dynamics of magnetic particles is described by the Landau–Lifshitz equation and its generalizations.[31–33] These kinds of equations have strong nonlinearities, and, therefore, complex dynamical behaviors are to be expected.[34–60] In particular, when the magnetic field is time-dependent, chaotic states[34] and period-doubling bifurcations,[45] as well as chaotic transients,[50] have been numerically observed. Moreover, two-dimensional phase diagrams based on Lyapunov exponents have been calculated finding complex transitions among periodic, quasi-periodic, and chaotic states,[62,63] as well as shrimp structures.[14] Recently, chaotic states due to driven pumping in a mono-domain regime have been experimentally found.[61] Nevertheless, to the best of our knowledge, a systematic study of the periodicity in magnetic systems has not been provided.[64]

The aim of the paper is to analyze numerically the periodicity of the magnetization dynamics of an anisotropic magnetic particle in the presence of a time-dependent magnetic field that has a harmonic as well as a constant term. We compute several Lyapunov and isospikes diagrams as a function of the driven amplitudes and frequency and as a function of the anisotropy's coefficients. Due to the complexity of the diagrams, iterative zooms are applied, and bifurcation diagrams are analyzed for specific lines in the parameter space. The article is organized as follows: In Sec. II, the model for the magnetization dynamics is presented. In Sec. III, the numerical analysis is performed, and the corresponding discussions are provided. Brief remarks are finally given in Sec. IV.

II. MAGNETIZATION DYNAMICS

Let us suppose that a magnetic particle is represented by a magnetic monodomain,[32,61] such that its magnetization is depicted by a magnetization vector $\mathbf{M} = \mathbf{M}(t)$. The evolution of the magnetization is determined by the dimensionless Landau–Lifshitz–Gilbert (LLG) equation,

$$\kappa \frac{d\mathbf{m}}{d\tau} = -\mathbf{m} \times \mathbf{h}_{eff} - \alpha \mathbf{m} \times (\mathbf{m} \times \mathbf{h}_{eff}), \quad (1)$$

where $\mathbf{m} = \mathbf{M}/M_s$, $\tau = t|\gamma|M_s$, and $\kappa = 1 + \alpha^2$. Here, γ is the gyromagnetic factor, which is associated with the electron spin and its numerical value is $|\gamma| = |\gamma_e|\mu_0 \approx 2.21 \times 10^5\,\mathrm{mA^{-1}\,s^{-1}}$ and M_s is the saturation magnetization. This scaling of the variables leads to $|\mathbf{m}| = 1$, which is a conserved quantity of the system.

Additionally, α denotes the dimensionless phenomenological dissipation coefficient, which is a property of the magnetic material. Representative orders of magnitude are 10^{-4} to 10^{-3} in garnets or 10^{-2} or greater for cobalt, nickel, or permalloy ($Ni_{80}Fe_{20}$).[32,64] An experimental value of the saturation magnetization is, for example, $M_{s[\mathrm{Co}]} \approx 1.42 \times 10^6$ A/m ≈ 17.8 kOe for cobalt based materials, implying that time scale is $(|\gamma|M_{s[\mathrm{Co}]})^{-1} \approx 3$ ps. In the case of magnetic materials with less saturation magnetization, one can increase the time scale, like in the case of Nickel nanoparticles.

The effective field, $\mathbf{h}_{eff}$, is given by

$$\mathbf{h}_{eff} = \mathbf{h}_{AP} + \sum_{j=1}^{3} \beta_j (\mathbf{m} \cdot \widehat{\mathbf{n}}_j)\widehat{\mathbf{n}}_j, \quad (2)$$

where $\mathbf{h}_{AP}$ is the external magnetic field and the coefficient β_j measures anisotropy along the axis $\mathbf{n}_j$. Here, the subindexes $j = (1, 2, 3)$ represent the main axes, denoted by the Cartesian coordinates as (x, y, z). We applied an external magnetic field $\mathbf{h}_{AP}$ composed by two terms, a constant longitudinal term and a periodical transversal term with fixed frequency and amplitude,

$$\mathbf{h}_{AP} = \mathbf{h}_0 + \mathbf{h}_T \sin(\Omega\tau + \phi), \quad (3)$$

where $\mathbf{h}_0$ $(\|\widehat{\mathbf{z}})$, $\mathbf{h}_T$ $(\perp \widehat{\mathbf{z}})$, Ω are time-independent, and ϕ is a constant phase. The dimensionless field and frequency are $\mathbf{h} = \mathbf{H}/M_s$ and $\Omega = \omega/(\gamma M_s)$ respectively. The field amplitude and frequency can be expressed as a function of M_s and (γM_s), respectively. Common values for the amplitude and frequencies are in the range of 10^0–10^1 kOe and GHz, respectively.[50,55,61] We choose to vary those parameters according to their experimental range values.

The second term of the right side of Eq. (2) corresponds to the anisotropy field. This term takes into account the fact that the magnetic properties depend on the direction that are measured.[65] This term is due to several factors as the crystalline, magnetoelastic, or the shape anisotropy. We remark that the effect of the anisotropies strongly modifies the dynamical behavior of the magnetic particles.[14,54]

III. NUMERICAL SIMULATIONS

In this section, we explore through intensive numerical simulations the dynamics of Eq. (1). Let us note that because we have a time-dependent magnetic field, the system is non-autonomous. To write the system in autonomous form, the LLG equation is first projected onto Cartesian coordinates, then a new variable is introduced by the transformation $W = \Omega\tau$. This produces an extra differential equation $dW/d\tau = \Omega$ for the new variable W. Therefore, the system is converted into an autonomous four-dimensional dynamical system. Equation (1) conserves its norm ($|\mathbf{m}| = 1$); consequently, the effective dimension is three. In Cartesian representation, the corresponding autonomous system can be explicitly written as

$$\begin{aligned}
\kappa \frac{dm_x}{d\tau} &= -h_z m_y + m_y m_z \beta_y - m_y m_z \beta_z + h_y m_z \sin(W+\phi) \\
&\quad - \alpha \Big[h_z m_x m_z - m_x m_y^2 \beta_x - m_x m_z^2 \beta_x + m_x m_y^2 \beta_y + m_x m_z^2 \beta_z \\
&\quad + h_y m_x m_y \sin(W+\phi) - h_x m_y^2 \sin(W+\phi) \\
&\quad - h_x m_z^2 \sin(W+\phi) \Big], \\
\kappa \frac{dm_y}{d\tau} &= h_z m_x - m_x m_z \beta_x + m_x m_z \beta_z - h_x m_z \sin(W+\phi) \\
&\quad - \alpha \Big[h_z m_y m_z + m_x^2 m_y \beta_x - m_x^2 m_y \beta_y - m_y m_z^2 \beta_y + m_y m_z^2 \beta_z \\
&\quad - h_y m_x^2 \sin(W+\phi) + h_x m_x m_y \sin(W+\phi) \\
&\quad - h_y m_z^2 \sin(W+\phi) \Big], \\
\kappa \frac{dm_z}{d\tau} &= m_x m_y \beta_x - m_x m_y \beta_y - h_y m_x \sin(W+\phi) + h_x m_y \sin(W+\phi) \\
&\quad - \alpha \Big[-h_z m_x^2 - h_z m_y^2 + m_x^2 m_z \beta_x + m_y^2 m_z \beta_y - m_x^2 m_z \beta_z \\
&\quad - m_y^2 m_z \beta_z + h_x m_x m_z \sin(W+\phi) + h_y m_y m_z \sin(W+\phi) \Big].
\end{aligned}$$

$$\frac{dW}{d\tau} = \Omega. \quad (4)$$

This system is numerically integrated using a fourth-order Runge–Kutta method with a fixed time step of $\delta\tau = 0.01$. The dynamic behavior of the magnetic particle is mainly described by three types of dynamical indicators: the largest Lyapunov exponents,[5] the technique of isospike diagrams,[15,16] and in the case of regular states, the period distribution. Finally, bifurcation diagrams[1] are used as a complementary indicator.

The Lyapunov exponents quantify the divergence between two initially close trajectories of the vector field. Therefore, they are used to determine chaotic and regular regions. They are denoted by λ_j and are ordered in descending manner, $\lambda_1 > \lambda_2 > \cdots > \lambda_N$, with λ_1 being the largest Lyapunov exponent (LLE). Since the effective dimension of the system is three, the LLE is powerful enough to analyze the chaotic regimes. If LLE is positive ($\lambda_1 > 0$), the state is chaotic, while if it is negative or zero ($\lambda_1 \leqslant 0$) the states are regular. Detailed works on the calculation of the exponents and their applications can be found in Refs. 1, 4, 7, and 66–70. In the following diagrams of the largest Lyapunov exponent, positive values that represent chaotic states are depicted in color code, while regular states are depicted in black.

On the other hand, to obtain the isospike diagrams, that is, to find the number of peaks per period of the oscillations, we first calculate the Lyapunov exponents and perform the integrations for 3×10^5 time steps, recording the maximums (or minimums) of the time series of the magnetization vector of each component, and check whether the peaks are repeated or not. In most of the cases, we use a palette of 16 colors to represent the number of peaks contained in a period of oscillations, as indicated by the color bars in the figures. States with more than 16 peaks are drawn in gray. The black color represents chaotic states. An advantage of the isospike diagrams is that they may also be systematically implemented to work with experimental data.[17,21] Moreover, to compute the period of each time series, we calculate the Fourier transform of each component and estimate the oscillation period from the Fourier spectrum. Here, the Fourier transform of the magnetization component m_j will be denoted as $\mathcal{F}_{m_j}(f)$, where f is its frequency with $j = (x, y, z)$. Furthermore, the precision is improved by performing a linear interpolation near the highest peak in the Fourier spectrum. This allows determining the oscillation period accurately and then a comparison is done with the period obtained by the isospike method.

Due to the large number of parameters, we fix the damping coefficient at $\alpha = 0.05$ in all the simulations. Besides, in most of the cases, we fix the phase in the driving field at $\phi = 0$. The rest of the parameters are varied to study their influence on dynamical behavior. We find that small variations of the different parameters as the magnetic field components, frequency, or anisotropy coefficients imply significative changes in the periodicity of the system. All two-dimensional phase diagrams have a resolution of 2000×2000 points in the parameter space, such that the points are equidistant. In Subsections III A–III C, the influences of those parameters are analyzed in detail.

A. Effects of the applied field

Figure 1 presents the largest Lyapunov exponent phase diagram and the corresponding isospike diagrams for the components m_x, m_y, and m_z as a function of the oscillatory field amplitude h_x and the frequency Ω. Note that different color codes are applied for LLE and the isospikes diagrams. As Fig. 1 shows, when comparing the two types of diagrams, both provide the same essential information: they precisely distinguish between chaos and periodicity. However, the isospikes diagrams are more informative. They show how the time series change in regions where the system presents different periods.

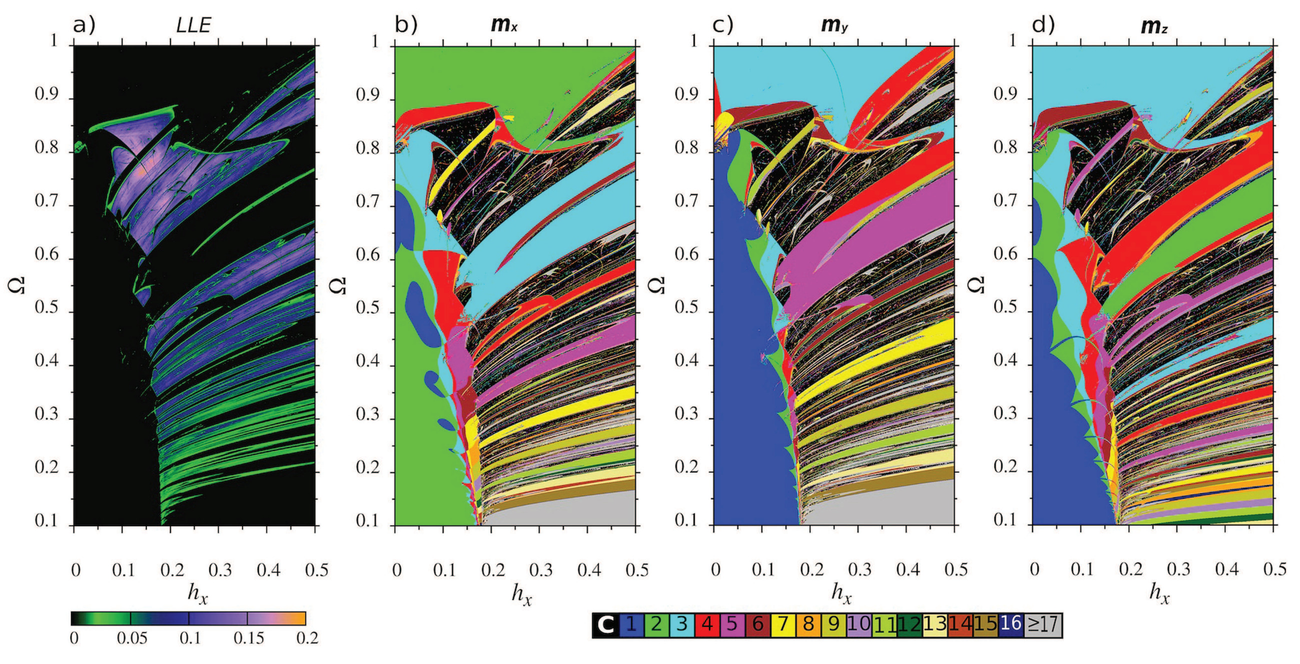

FIG. 1. Phase diagrams in color code as a function of the frequency Ω and the driven field amplitude h_x. Panel (a) represents the largest Lyapunov exponent. Frames (b), (c), and (d) correspond to the isospike diagrams for the magnetization components (m_x, m_y, m_z), respectively. The fixed parameters are $h_y = 1.0$, $h_z = 4.0$, $\phi = 0$, $\beta_x = 4.0$, $\beta_y = 0.0$, $\beta_z = -1.0$, and $\alpha = 0.05$.

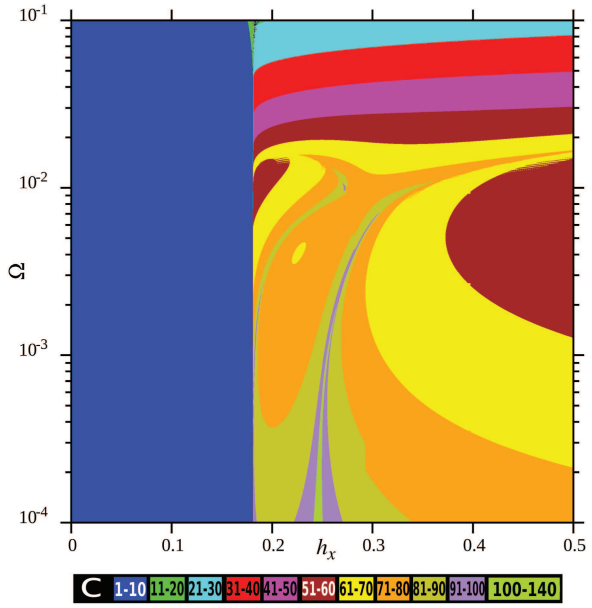

FIG. 2. Isospike diagram for the m_x component as a function of the frequency Ω and the field amplitude h_x. The fixed parameters are: $h_y = 1.0$, $h_z = 4.0$, $\phi = 0$, $\beta_x = 4.0$, $\beta_y = 0.0$, $\beta_z = -1.0$, and $\alpha = 0.05$. Here, the range of the frequency takes small values and its scale is logarithmic.

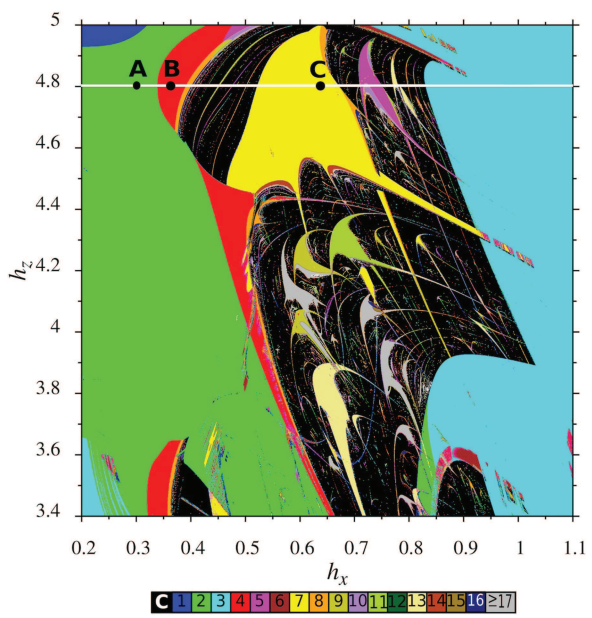

FIG. 3. Isospike diagram for the m_x component as a function of the field amplitudes h_z and h_x. The fixed parameters are $\Omega = 1.0$, $\beta_x = 4.0$, $\phi = 0$, $\beta_y = 0.0$, $\beta_z = -1.0$, $h_y = 1.0$, and $\alpha = 0.05$.

We consider a three-dimensional model for the magnetic moment; Figs. 1(b), 1(c), and 1(d) show the isospikes diagrams for the components m_x, m_y, and m_z, respectively. It shows that the distribution of the registered peaks depends largely on the component. Hence, changes in the regular phases of the isospikes diagram are expected when different components are analyzed. Although they show similar structures, the specific details of each diagram depend on the dynamical variable considered.

Furthermore, these diagrams also show that chaos occurs only above a certain field strength h_x. Indeed, chaos first appears at a finite frequency, which corresponds roughly to the characteristic time scale of magnetization dynamics. For smaller frequencies, the field amplitude has to be large to experience chaos. Small frequencies $\Omega < 0.1$ make the appearance of chaos difficult. Besides, as the number of peaks increases, the frequency decreases above a certain field strength h_x. The increment in the number of peaks is due to the lower frequency and above a threshold field value. The system shows a reversal of the magnetization in the component m_x, caused by the oscillating field h_x. When the field is oscillating and exceeds the threshold value at low frequency, the system reverses the component m_x at $h_x > 0$. If the field takes values less than zero, m_x reverts and oscillates around zero values. The number of oscillations increases as the frequency decreases; therefore, the number of peaks will grow as well. However, for high frequencies, the reversion time decreases; this causes the magnetization vector to perform little or no oscillation with the corresponding decrease in the number of peaks. For h_x lower than the threshold value and low frequencies, the field strength is not enough to reverse the m_x component, reducing also the number of peaks. If in a certain region of the diagram, the three components of the magnetization vector oscillate with a single peak, which is represented by blue color in the isospike diagrams, then the system is synchronized with the field. Hence, we can observe synchronization islands with the same period appearing at field values below a certain intensity.

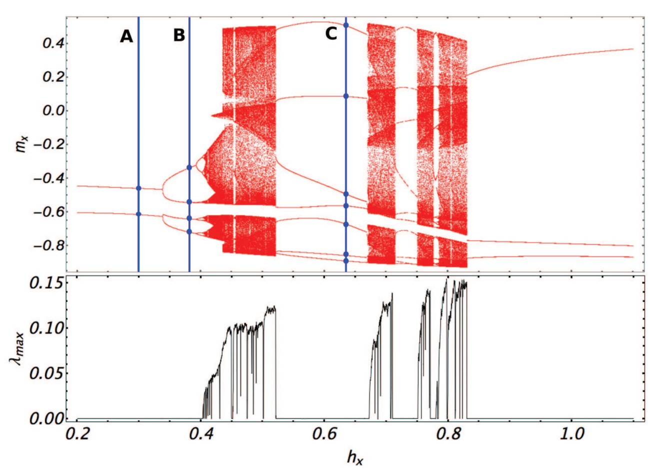

FIG. 4. Bifurcation diagram of the m_x component and the largest Lyapunov exponent as a function of h_x for the line marked in Fig. 3 at $h_z = 4.8$.

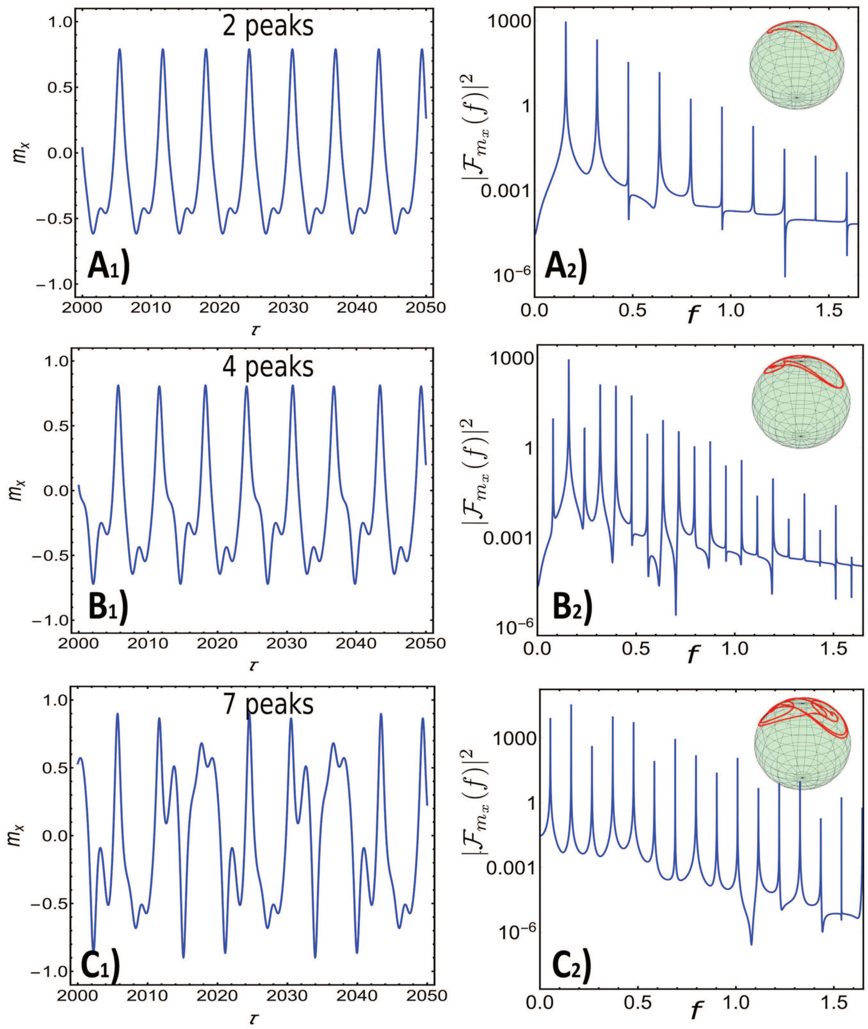

FIG. 5. Time series of the m_x component and their corresponding amplitude of Fourier transform for the points marked in Fig. 4. The insets in the Fourier spectrum show 3D phase diagrams of the magnetization components. The corresponding field values are $h_x = 0.30$, $h_x = 0.38$, and $h_x = 0.64$, respectively.

Let us also remark that when the frequency Ω takes smaller values, most states are regular with higher periodicity. To illustrate this phenomenon, Fig. 2 shows the phase diagram in color code of the isospike for the m_x component as a function of Ω and h_x. Here, the range of Ω is between 10^{-4} and 10^{-1}, and the scale is chosen as logarithmic. The rest of the parameters are the same as in Fig. 1. We note that only a small portion of the figure, close to region $0.18 < h_x < 0.19$ and $0.05 < \Omega < 0.1$, exhibits chaotic states. Besides, we can observe that the system presents higher periodicities, such that the number of peaks increases substantially in comparison with what occurs for larger values of Ω. Indeed, the color code used in this figure to measure the isospikes has a range of tens instead of unity. Let us comment that to compute this diagram, the integration time has been increased to 2×10^6 time steps after the transient. More details on this figure can be found in the supplementary material of the article.

Interesting results are presented when both the static and driven field amplitudes h_z and h_x are varied simultaneously as shown in Fig. 3. The isospike diagram of the m_x component shows some well-known structures of the dynamic systems, the so-called *shrimps*,[6] depicted in the center of the two panels of the figure. As it can be seen in the isospike diagrams, the shrimps are complex structures composed of an infinite succession of periodic oscillations immerse in a chaotic phase. As the number of peaks grows, a striking feature is distorted more and more, as the periodic field amplitude increases. The regular phases have a rather complex organization, invaded by shrimp sequences, that is, by sequences of islands in which high periodicity behavior are found and with a high number of peaks per period. In addition, the phase diagram shows well-defined boundaries when the transition between the number of peaks occurs and where the shrimp sequences accumulate. In the phase diagram, we can see specific points marked and a white line for $h_z = 4.8$; along this line, the bifurcation diagram for the component m_x is shown in the upper panel of Fig. 4. The lower panel shows the LLE as a function of h_x. All branching diagrams were calculated by scanning the white line from left to the right, always starting

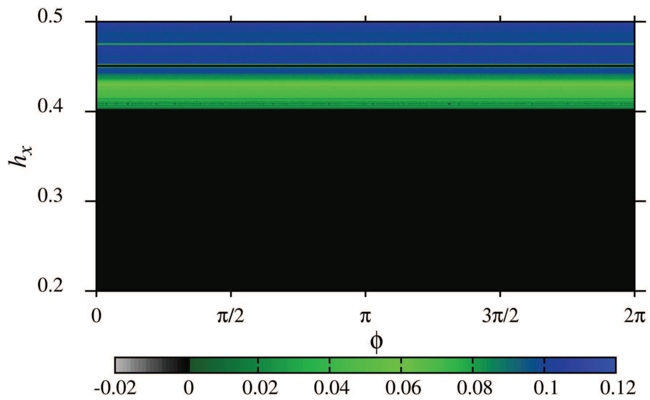

FIG. 6. Phase diagrams of the largest Lyapunov exponent in color code as a function of the phase ϕ and the driven field amplitude h_x. The fixed parameters are $h_y = 1.0$, $h_z = 4.8$, $\Omega = 1.0$, $\beta_x = 4.0$, $\beta_y = 0$, $\beta_z = -1.0$, and $\alpha = 0.05$.

with the same fixed initial condition and showing the evolution of the local peaks, of the m_x component. For a better understanding, it contains blue lines that delimit specific points in the phase diagram; each intersection with a branch of the bifurcation diagram is marked by a point. This point denotes a maximum (or a minimum) of the time series; hence, the number of intersects represents the number of peaks per period. In both cases, the bifurcation diagram shows a clear coincidence of the information provided by the Lyapunov exponents and the isospike diagram. It can be also seen that the route to chaos for $0.30 < h_x < 0.40$ is through period-doubling cascades. The region between $0.40 < h_x < 0.84$ shows a window in which periodic and chaotic dynamics are intermingled, inside a continuum of the branches of the bifurcation diagram whenever $\lambda_1 = 0$ is observed. Moreover, when $\lambda_1 > 0$, the chaotic behavior is denoted by windows with diffused points. Finally, when $h_x > 0.84$, one observes a periodic region with time series containing three peaks.

Figure 5 shows the time series for the m_x, and the corresponding amplitude of the Fourier transform as a function of the frequency, f, for particular cases of h_x taken at the specific values corresponding to the vertical lines denoted by the letters **A**, **B**, and **C** in Fig. 4. We can observe in the panels how the peaks are deformed, presenting slight distortions. They present an increase in the period as the number of spikes increases. The time series illustrates a complex periodic dynamics. Besides, we can infer from the Fourier spectrum that the states are periodic. In the three cases, the frequencies are commensurate. We always have the fundamental frequency and the harmonics and sometimes sub-harmonics peaks with respect to the forcing frequency. We emphasize that we have not found quasi-periodic states in this range of parameters. Indeed, quasi-periodic states would have incommensurate peaks in the Fourier spectrum.

Let us also analyze the effect of the phase in the driving field, ϕ. Figure 6 shows the largest Lyapunov exponent color coded as a function of the phase ϕ and the driven field amplitude h_x. We observe that only small changes appear as a function of the phase, ϕ. We also recognize that when the field increases, chaotic bands are present. On the contrary, for values $h_x \lesssim 0.4$, only regular states are found.

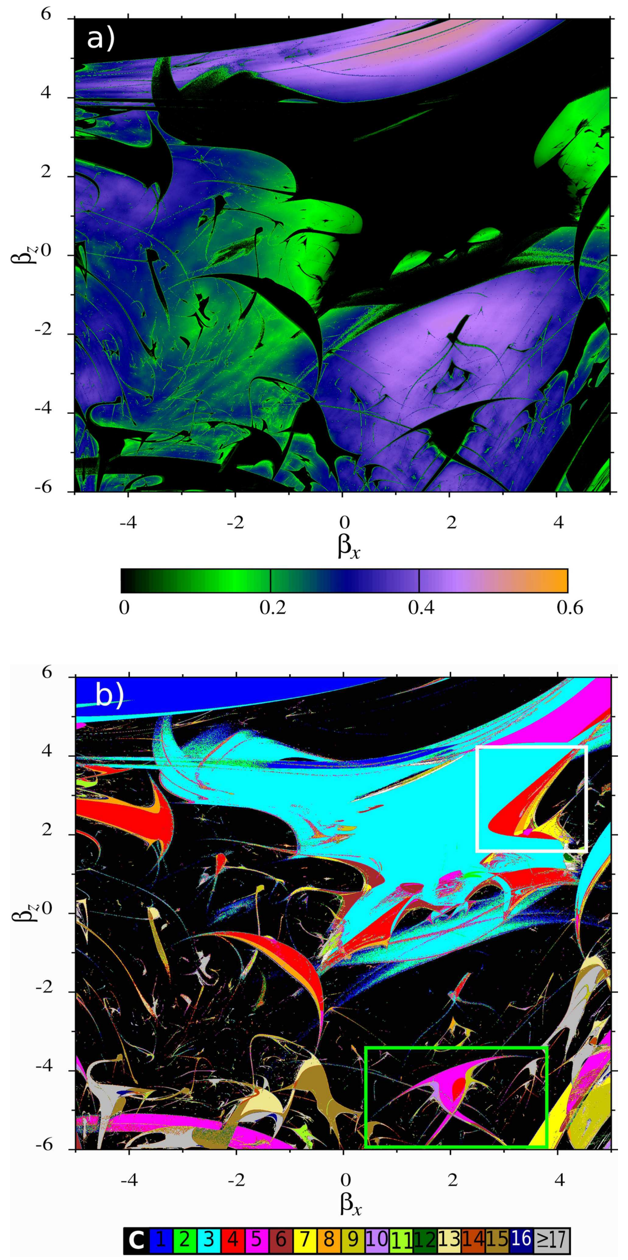

FIG. 7. Phase diagrams as a function of the anisotropy coefficients β_z and β_x. (a) Representation in terms of the LLE. (b) Isospike diagram for m_x component. The fixed parameters are $\Omega = 1.0$, $h_x = 2.45$, $h_y = 2.45$, $h_z = 0.10$, $\phi = 0$, $\beta_y = 2.0$, and $\alpha = 0.05$.

B. Effect of anisotropy

In order to explore in more detail the influence of the material's parameters on the chaotic and regular states, we focus, in particular, on the effect of anisotropy. Figure 7 displays phase diagrams based

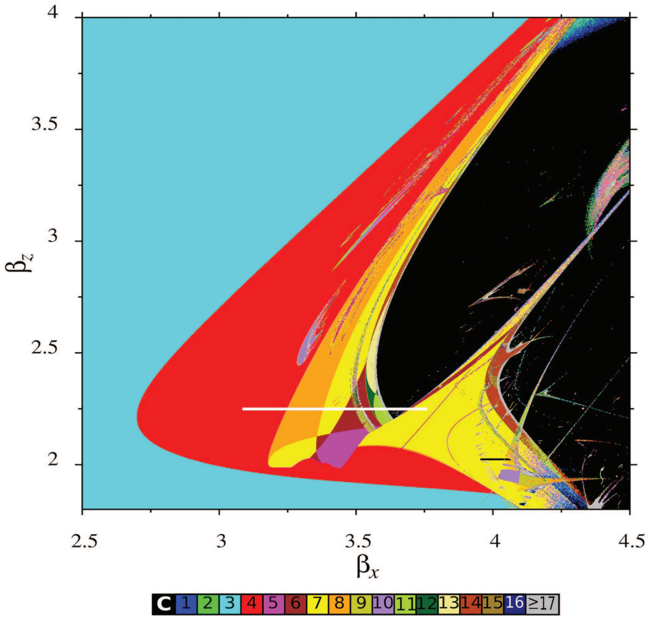

FIG. 8. Isospikes diagram for the m_x component of the region enclosed by the white rectangle in Fig. 7.

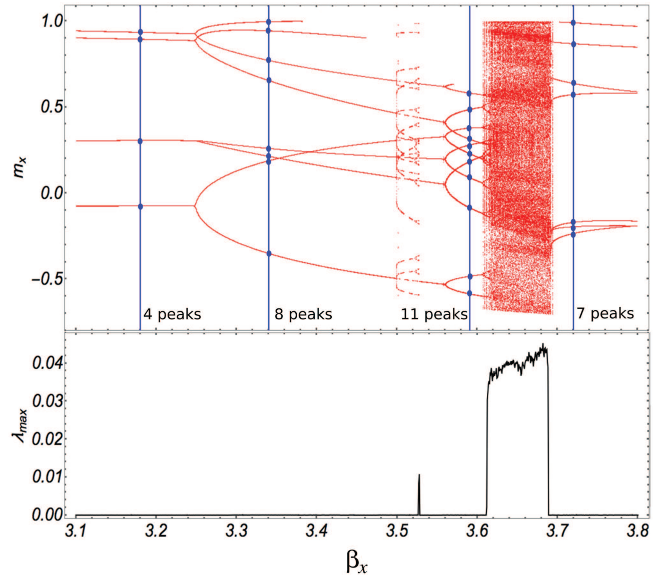

FIG. 9. Bifurcation diagram of the m_x component and the largest Lyapunov exponent as a function of β_x for the line marked in Fig. 8 at $\beta_z = 2.25$.

on the largest Lyapunov exponent and the isospike diagram for the m_x as a function of β_z and β_x. As before, the phase diagram of the Lyapunov exponents shows good agreement with the information of the phase diagram based on the number of spikes per period. There is no trend or symmetry due to the effect of anisotropy, but shrimp-like structures appear as mentioned above. In the upper diagram, the black regions represent regular islands embedded in the chaotic sea. For positive values of both constants (β_x, β_z), we observe a predominance of regular behavior. For a deeper insight, we perform the isospike diagram at the lower panel. Here, we analyze the periodicity of these regular islands finding that there exist multiple periodic regions with complex shapes. Indeed, to get more information, we have chosen two interesting areas and performed the iterative zooms shown in Fig. 8. The green box contains a typical shrimp delimited by $0.5 < \beta_x < 3.8$ and $-6 < \beta_z < -3$, while the white box between $2.2 < \beta_x < 5$ and $1.8 < \beta_z < 4.2$ contains a succession of different periods depicted in Fig. 8. Note that this fact is not reflected in the upper diagram; therefore, the analysis of these kinds of features with isospike diagrams becomes a powerful tool.

Figure 8 shows an enlarged view of the white rectangle of Fig. 7. The transition between different periodicities with clearly defined borders is recognized. In the largest area, the system presents three spikes, while the second one has four spikes. After several transitions of regions with different periodicities, an abrupt transition to chaos is observed. This is confirmed by the bifurcation diagram of the m_x component shown in Fig. 9. The bifurcation diagram fits perfectly with in the LLE, with the difference that the branches are not continuous, which can be an effect of anisotropy. Again, between $\beta_x = 3.6$ and $\beta_x = 3.7$ ($\lambda_1 > 0$) a diffuse point window appears, which is a hallmark of chaotic behavior. Let us also remark that the effect of anisotropy causes an increase of the number of peaks when $\beta_x < 3.6$. Nevertheless, for $\beta_x > 3.7$, the number of peaks decreases. This variation is different from that caused by the effect of the field h_x due to the magnetic reversal; in this case, the m_x component oscillates around positive values without a full reversal change. Note that in the case of Fig. 4(a), the bifurcation diagram is constructed by following the values of the local minima (dips). On the contrary, the bifurcation diagram of Fig. 9 is constructed with the local maxima (peak values). This is just an esthetic choice because either option is a valid choice for constructing a bifurcation diagram.

Figure 10 shows the isospikes diagrams for the three magnetization components (m_x, m_y, m_z). Similar characteristics are presented as described above. In particular, the peaks of m_y and m_z produce a similar diagram to the m_x one. In panels (a) and (b), it is easy to recognize that, although the variables m_x and m_y oscillate differently, the general structure of the diagrams is the same, the difference being simply in the number of peaks per period. Since the system contains a constraint, $|\mathbf{m}| = 1$, there is a link among the three components in the number of the spikes. Furthermore, the presence of shrimps that appears stretched in various forms can be observed with an internal structure composed of more than one period.

Finally, a new type of phase diagram is shown at the bottom right side of Fig. 10(d). In this panel, the period distribution is presented, such that the parameters are in color coding according to the period of their corresponding oscillations. Chaotic states are shown in black. As evident, period diagrams can also reveal details of the substructures that form periodicity islands.

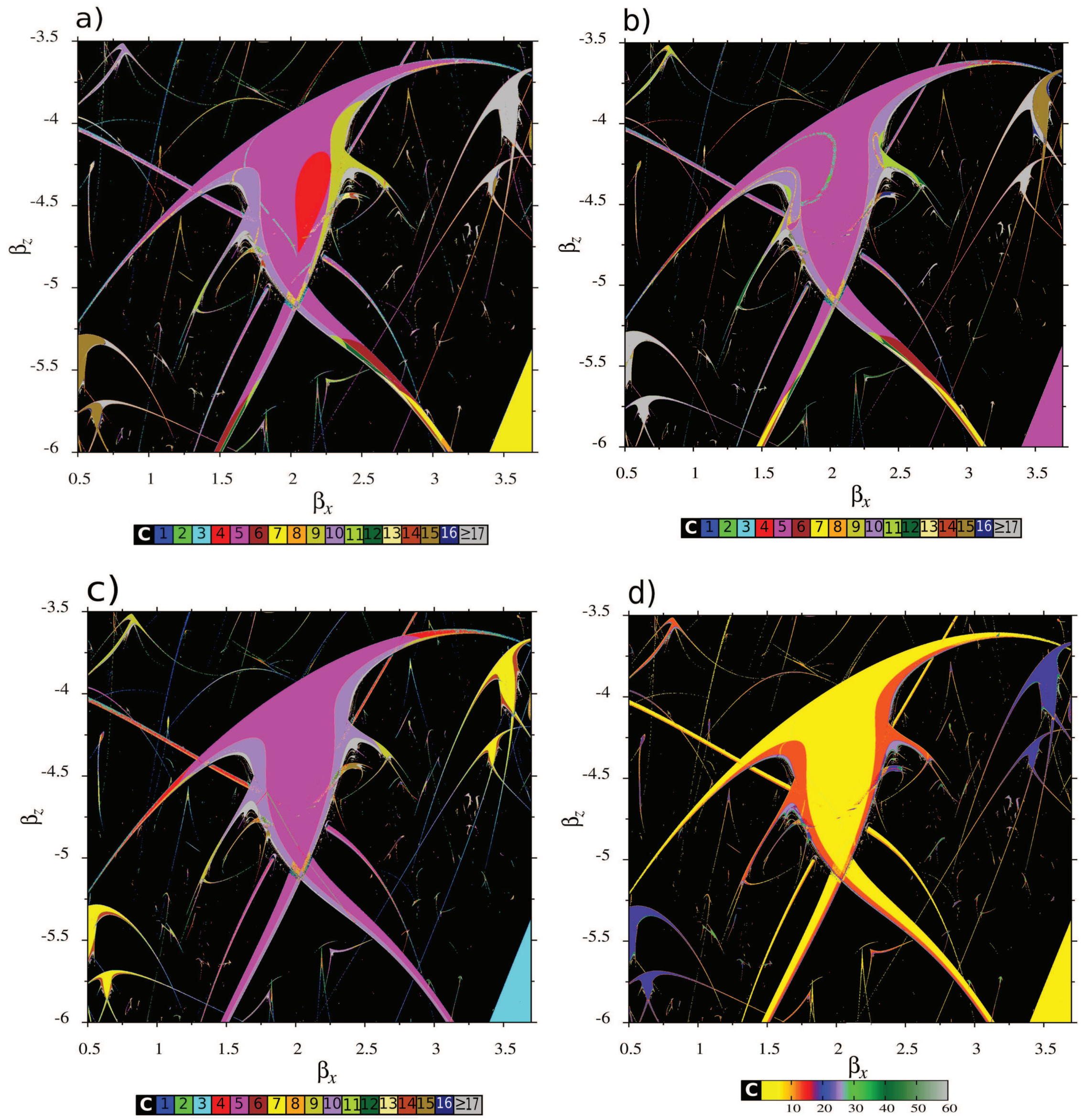

FIG. 10. Phase diagrams for the region enclosed by the green rectangle in Fig. 7. Frames (a)–(c) show the isospike diagrams for the components m_x, m_y, and m_z, respectively. Frame (d) shows the period distribution diagram, in which chaotic states are depicted in black.

However, to reveal greater details in this kind of graph, it is usually necessary to define a higher cut-off period; more information can be found in Ref. 27. We can observe that most of the central shrimp structure has lower values of the periods, while in both edges, the periods increase their values in a symmetric fashion. The fundamental period is directly related to the Ω value, the forcing angular frequency. Indeed, if $\Omega = 1$, then the period is $T = 2\pi/\Omega \approx 6.28$. However, we see in Fig. 10(d) that only the central part of the shrimp structure corresponds to the fundamental period $T \approx 6.28$. On the edges of the structure, the period is increased, which indicates that the actual observed frequency is decreased with respect to the angular forcing frequency. Hence, at the edges of shrimp, the states are periodic but we observe sub-harmonic responses with respect to the forcing frequency.

C. Effect of initial conditions

Since the system is nonlinear, multiple stable solutions can be found depending on the initial conditions for the same fixed

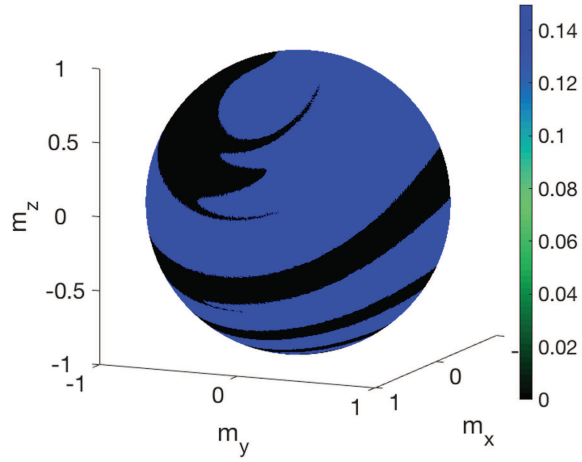

FIG. 11. 3D phase diagram of (m_x, m_y, m_z) for 10^6 different initial conditions. The color code indicates the resulting LLE, such that green-blue regions indicate a chaotic regime and the black regions indicate a periodic one. The fixed parameters are $h_y = 0.82$, $h_y = 1.0$, $h_z = 4.0$, $\phi = 0$, $\beta_x = 4.0$, $\beta_y = 0.0$, $\beta_z = -1.0$, and $\alpha = 0.05$.

parameters. We illustrate this interesting phenomenon in the LLG equation. We started Eq. (1) with 10^6 different initial conditions covering the unit sphere for the fixed values of parameters of Fig. 5 at $h_x = 0.82$. Figure 11 shows a 3D phase diagram of (m_x, m_y, m_z), and the color code indicates the resulting LLE. The black regions correspond to periodic regimes, and the green-blue regions refer to chaotic ones. Multi-stability is observed, between regular and chaotic states. Additional details are provided in the supplementary material on the multi-stability question.

IV. FINAL REMARKS

Numerical simulations of the magnetization dynamics of a magnetic particle using isospike diagrams show that a time-dependent magnetic field induces states with different periodicity. The transitions between regular states with different periodicity delimit well-defined boundaries in the parameter space. For example, in certain cases, the transition between regular and chaotic states is achieved by a period-doubling cascade. The isospike diagrams reveal the existence of significative differences in the dynamical behavior of the system when varying the different parameters. Indeed, when the applied fields h_x and h_z are varied, the evolution of the time series is different from the evolution produced by the variation of the anisotropy coefficients β_x and β_z. Furthermore, we can distinguish shrimp shaped topological structures with inner parts that may or may not present different periodicities. This fact is of great importance due to the numerous reports mentioning these structures in different dynamical systems.[15,21,25,71] Although there are many studies concerning chaos in magnetic systems, we want to emphasize that the understanding and characterization of the periodicity windows is of great relevance.

SUPPLEMENTARY MATERIAL

See the supplementary material for the complementary information concerning LLE and isospike phase diagrams as a function of Ω and h_x for the low-frequency regime and to explore the effect in more detail of the initial conditions.

ACKNOWLEDGMENTS

L.M.P. and D.L. acknowledge partial financial support from the FONDECYT (No. 1180905). D.L. acknowledges partial financial support from the Centers of Excellence with BASAL/CONICYT financing (Grant No. AFB180001), CEDENNA. J.B. acknowledges partial financial support from the Spanish Ministry of Science and Technology under Contract No. SAF2017-88019-C3-2-R.

DATA AVAILABILITY

The data that support the findings of this study are available from the corresponding author upon reasonable request.

REFERENCES

[1] J. C. Sprott, *Chaos and Time-Series Analysis* (Oxford University Press, UK, 2003).
[2] H. Kantz and T. Schreiber, *Nonlinear Time Series Analysis* (Cambridge University Press, 2010).
[3] S. Boccaletti, C. Grebogi, Y. C. Lai, H. Mancini, and D. Maza, "The control of chaos: Theory and applications," Phys. Rep. **329**, 103–197 (2000).
[4] *Chaos Detection and Predictability*, edited by C. H. Skokos, G. A. Gottwald, and J. Laskar (Springer, 2016).
[5] A. Wolf, J. B. Swift, H. L. Swinney, and J. A. Vastano, "Determining Lyapunov exponents from a time series," Physica D **16**, 285 (1985).
[6] J. A. Gallas, "Structure of the parameter space of the Hénon map," Phys. Rev. Lett. **70**, 2714 (1993).
[7] J. A. C. Gallas, "The structure of infinite periodic and chaotic hub cascades in phase diagrams of simple autonomous flows," Int. J. Bifurc. Chaos **20**, 197 (2010).
[8] Y. Zou, M. Thiel, M. C. Romano, and J. Kurths, "Shrimp structure and associated dynamics in parametrically excited oscillators," Int. J. Bifurc. Chaos **16**, 3567–3579 (2006).
[9] H. R. Dullin, S. Schmidt, P. H. Richter, and S. K. Grossmann, "Extended phase diagram of the Lorenz model," Int. J. Bifurc. Chaos **17**, 3013–3033 (2007).
[10] R. Barrio, F. Blesa, and S. Serrano, "Topological changes in periodicity hubs of dissipative systems," Phys. Rev. Lett. **108**, 214102 (2012).
[11] W. Façanha, B. Oldeman, and L. Glass, "Bifurcation structures in two-dimensional maps: The endoskeletons of shrimps," Phys. Lett. A **377**, 1264–1268 (2013).
[12] T. Xing, R. Barrio, and A. Shilnikov, "Symbolic quest into homoclinic chaos," Int. J. Bifurc. Chaos **24**, 1440004 (2014).
[13] R. Barrio, M. Á. Martínez, S. Serrano, and D. Wilczak, "When chaos meets hyperchaos: 4D Rössler model," Phys. Lett. A. **379**, 2300–2305 (2015).
[14] L. M. Pérez, J. Bragard, H. L. Mancini, J. A. C. Gallas, A. M. Cabanas, O. J. Suarez, and D. Laroze, "Anisotropy effects on magnetization dynamics," Net. Het. Med. **10**, 209 (2015).
[15] M. A. Nascimento, J. A. Gallas, and H. Varela, "Self-organized distribution of periodicity and chaos in an electrochemical oscillator," Phys. Chem. Chem. Phys. **13**, 349–784 (2011).
[16] J. G. Freire and J. A. C. Gallas, "Stern–Brocot trees in the periodicity of mixed-mode oscillations," Phys. Chem. Chem. Phys. **13**, 12191 (2011).
[17] A. Sack, J. G. Freire, E. Lindberg, T. Pöschel, and J. A. C. Gallas, "Discontinuous spirals of stable periodic oscillations," Sci. Rep. **3**, 3350 (2013).
[18] M. R. Gallas, M. R. Gallas, and J. A. C. Gallas, "Distribution of chaos and periodic spikes in a three-cell population model of cancer," Eur. Phys. J. Spec. Top. **223**, 2131–2144 (2014).

[19] J. Park, H. Lee, Y. Jeon, and J. Baik, "Periodicity of the Lorenz–Stenflo equations," Phys. Scr. **90**, 065201 (2015).
[20] J. Park, H. Lee, and J. Baik, "Periodic and chaotic dynamics of the Ehrhard–Müller system," Int. J. Bifurc. Chaos **26**, 1630015 (2016).
[21] J. A. C. Gallas, "Spiking systematics in some CO_2 laser models," Adv. At. Mol. Opt. Phys. **65**, 127–191 (2016).
[22] S. Moon, B. Han, J. Park, J. M. Seo, and J. Baik, "Periodicity and chaos of high-order Lorenz systems," Int. J. Bifurc. Chaos **27**, 1750176 (2017).
[23] V. Wiggers and P. C. Rech, "Multistability and organization of periodicity in a Van der Pol–Duffing oscillator," Chaos Soliton. Fract. **103**, 632–637 (2017).
[24] V. Wiggers and P. C. Rech, "Chaos, periodicity, and quasiperiodicity in a radio-physical oscillator," Int. J. Bifurcation Chaos **27**, 1730023 (2017).
[25] P. C. Rech, "Organization of the periodicity in the parameter-space of a glycolysis discrete-time mathematical model," J. Math. Chem. **57**, 632–637 (2019).
[26] P. C. Rech, S. Dhua, and N. C. Pati, "Multistability and bubbling route to chaos in a deterministic model for geomagnetic field reversals," Int. J. Bifurc. Chaos **29**, 1930034 (2019).
[27] J. A. Gallas, "Stability diagrams for a memristor oscillator," Eur. Phys. J. Spec. Top. **228**, 2081 (2019), and reference therein.
[28] G. Ramírez, I. M. Jánosi, and J. A. Gallas, "Two-parameter areal scaling in the Hénon map," Europhys. Lett. **126**, 20001 (2019).
[29] J. G. Freire, A. Caldeórn, H. Varela, and J. A. Gallas, "Phase diagrams and dynamical evolution of the triple-pathway electro-oxidation of formic acid on platinum," Phys. Chem. Chem. Phys. **22**, 1078–1091 (2020).
[30] M. N. Mahmud, Z. Siri, J. A. Vélez, L. M. Pérez, and D. Laroze, "Chaotic convection in an Oldroyd viscoelastic fluid in saturated porous medium with feedback control," Chaos **30**, 073109 (2020).
[31] *Nonlinear Phenomena and Chaos in Magnetic Materials*, edited by P. E. Wigen (World Scientific, Singapore, 1994).
[32] G. Bertotti, I. Mayergoyz, and C. Serpico, *Nonlinear Magnetization Dynamics in Nanosystems* (Elsevier, Amsterdam, 2009).
[33] M. Lakshmanan, "The fascinating world of the Landau–Lifshitz–Gilbert equation: An overview," Phil. Trans. R. Soc. A **369**, 1280–1300 (2011).
[34] L. F. Alvarez, O. Pla, and O. Chubykalo, "Quasiperiodicity, bistability and chaos in the Landau–Lifshitz equation," Phys. Rev. B **61**, 11613 (2000).
[35] G. Bertotti, C. Serpico, and I. D. Mayergoyz, "Nonlinear magnetization dynamics under circularly polarized field," Phys. Rev. Lett. **86**, 724 (2001).
[36] P.-B. He and W. M. Liu, "Nonlinear magnetization dynamics in a ferromagnetic nanowire with spin current," Phys. Rev. B **72**, 064410 (2005).
[37] D. Laroze and P. Vargas, "Dynamical behavior of two interacting magnetic nanoparticles," Physica B **372**, 332 (2006).
[38] D. I. Sementsov and A. M. Shutyi, "Nonlinear regular and stochastic dynamics of magnetization in thin-film structures," Phys. Usp. **50**, 793 (2007).
[39] D. Laroze, P. Vargas, C. Cortes, and G. Gutierrez, "Dynamics of two interacting dipoles," J. Magn. Magn. Mater. **320**, 1440 (2008).
[40] D. Laroze and L. M. Perez, "Classical spin dynamics of four interacting magnetic particles on a ring," Physica B **403**, 473 (2008).
[41] P. P. Horley, V. R. Vieira, P. M. Gorley, V. K. Dugaev, and J. Barnas, "Influence of a periodic magnetic field and spin-polarized current on the magnetic dynamics of a monodomain ferromagnet," Phys. Rev. B **77**, 054427 (2008).
[42] D. V. Vagin and P. Polyakov, "Control of chaotic and deterministic magnetization dynamics regimes by means of sample shape varying," J. Appl. Phys. **105**, 033914 (2009).
[43] A. M. Shutyi and D. I. Sementsov, "Chaotic magnetization dynamics in single-crystal thin-film structures," Crystallogr. Rep. **54**, 98 (2009).
[44] A. M. Shutyĭ and D. I. Sementsov, "Regular and chaotic dynamics of magnetization precession in ferrite–garnet films," Chaos **19**, 013110 (2009).
[45] R. K. Smith, M. Grabowski, and R. E. Camley, "Period doubling toward chaos in a driven magnetic macrospin," J. Magn. Magn. Mater. **322**, 2127 (2010).
[46] Y. Khivintsev, B. Kuanr, T. J. Fal, M. Haftel, R. E. Camley, Z. Celinski, and D. L. Mills, "Nonlinear ferromagnetic resonance in permalloy films: A nonmonotonic power-dependent frequency shift," Phys. Rev. B **81**, 054436 (2010).
[47] Y. Khivintsev, J. Marsh, V. Zagorodnii, I. Harward, J. Lovejoy, P. Krivosik, R. E. Camley, and Z. Celinski, "Nonlinear amplification and mixing of spin waves in a microstrip geometry with metallic ferromagnets," Appl. Phys. Lett. **98**, 042505 (2011).
[48] D. Laroze, D. Becerra-Alonso, J. A. C. Gallas, and H. Pleiner, "Magnetization dynamics under a quasiperiodic magnetic field," IEEE Trans. Magn. **48**, 3567 (2012).
[49] D. Urzagasti, D. Becerra-Alonso, L. M. Pérez, H. L. Mancini, and D. Laroze, "Hyper-chaotic magnetisation dynamics of two interacting dipoles," J. Low Temp. Phys. **181**, 211 (2015).
[50] M. G. Phelps, K. L. Livesey, A. M. Ferona, and R. E. Camley, "Tunable transient decay times in nonlinear systems: Application to magnetic precession," Europhys. Lett. **109**, 37007 (2015).
[51] S. I. Denisov, T. V. Lyutyy, B. O. Pedchenko, and O. M. Hryshko, "Induced magnetization and power loss for a periodically driven system of ferromagnetic nanoparticles with randomly oriented easy axes," Phys. Rev. B **94**, 024406 (2016).
[52] P. Horley, M. Kushnir, M. Morales-Meza, A. Sukhov, and V. Rusyn, "Period-doubling bifurcation cascade observed in a ferromagnetic nanoparticle under the action of a spin-polarized current," Physica B **486**, 60 (2016).
[53] A. Pivano and V. O. Dolocan, "Chaotic dynamics of magnetic domain walls in nanowires," Phys. Rev. B **93**, 144410 (2016).
[54] A. M. Ferona and R. E. Camley, "Nonlinear and chaotic magnetization dynamics near bifurcations of the Landau–Lifshitz–Gilbert equation," Phys. Rev. B **95**, 104421 (2017).
[55] G. Okano and Y. Nozaki, "Evaluation of the effective potential barrier height in nonlinear magnetization dynamics excited by ac magnetic field," Phys. Rev. B **97**, 014435 (2018).
[56] A. M. Cabanas, L. M. Pérez, and D. Laroze, "Strange non-chaotic attractors in spin valve systems," J. Magn. Magn. Mater. **460**, 320–326 (2018).
[57] A. M. Ferona and R. E. Camley, "Nonlinear power-dependent effects in exchange-coupled magnetic bilayers," Phys. Rev. B **99**, 064405 (2019).
[58] J. Williame, A. D. Accioly, D. Rontani, M. Sciamanna, and J. Kim, "Chaotic dynamics in a macrospin spin-torque nano-oscillator with delayed feedback," Appl. Phys. Lett. **114**, 232405 (2019).
[59] T. Devolder, D. Rontani, S. Petit-Watelot, K. Bouzehouane, S. Andrieu, J. Letang, M. Yoo, J. Adam, C. Chappert, S. Girod, V. Cros, M. Sciamanna, and J. Kim, "Chaos in magnetic nanocontact vortex oscillators," Phys. Rev. Lett. **123**, 147701 (2019).
[60] C. Gibson, S. Bildstein, J. A. Lee, and M. Grabowski, "Nonlinear resonances and transitions to chaotic dynamics of a driven magnetic moment," J. Magn. Magn. Mater. **501**, 166352 (2020).
[61] E. Montoya, S. Perna, Y. Chen, J. A. Katine, M. d'Aquino, C. Serpico, and I. N. Krivorotov, "Magnetization reversal driven by low dimensional chaos in a nanoscale ferromagnet," Nat. Commun. **10**, 543 (2019).
[62] D. Laroze, J. Bragard, O. J. Suarez, and H. Pleiner, "Characterization of the chaotic magnetic particle dynamics," IEEE Trans. Magn. **47**, 3032 (2011).
[63] J. Bragard, H. Pleiner, O. J. Suarez, P. Vargas, J. A. C. Gallas, and D. Laroze, "Chaotic dynamics of a magnetic nanoparticle," Phys. Rev. E **84**, 037202 (2011).
[64] X. Batlle and A. Labarta, "Finite-size effects in fine particles: Magnetic and transport properties," J. Phys. D **35**, R15–R42 (2002).
[65] B. D. Cullity and C. D. Graham, *Introduction to Magnetic Materials*, 2nd ed. (John Wiley, 2009).
[66] S. Boccaletti, D. L. Valladares, J. Kurths, D. Maza, and H. Mancini, "Synchronization of chaotic structurally nonequivalent systems," Phys. Rev. E **61**, 3712 (2000).
[67] J. Bragard, G. Vidal, and H. Mancini, "Chaos suppression through asymmetric coupling," Chaos **17**, 043107 (2007).
[68] D. Laroze, P. G. Siddheshwar, and H. Pleiner, "Chaotic convection in a ferrofluid," Commun. Nonlinear Sci. Numer. Simul. **18**, 2436 (2013).
[69] D. Laroze and H. Pleiner, "Thermal convection in a nonlinear non-Newtonian magnetic fluid," Commun. Nonlinear Sci. Numer. Simul. **26**, 167 (2015).
[70] A. Pikovsky and A. Politi, *Lyapunov Exponents: A Tool to Explore Complex Dynamics* (Cambridge University Press, 2016).
[71] S. Moon, B. Han, J. Park, J. Seo, and J. Baik, "A physically extended Lorenz system," Chaos **29**, 063129 (2019).